RSC Advances

ROYAL SOCIETY OF CHEMISTRY

www.rsc.org/advances

Graphical Abstract

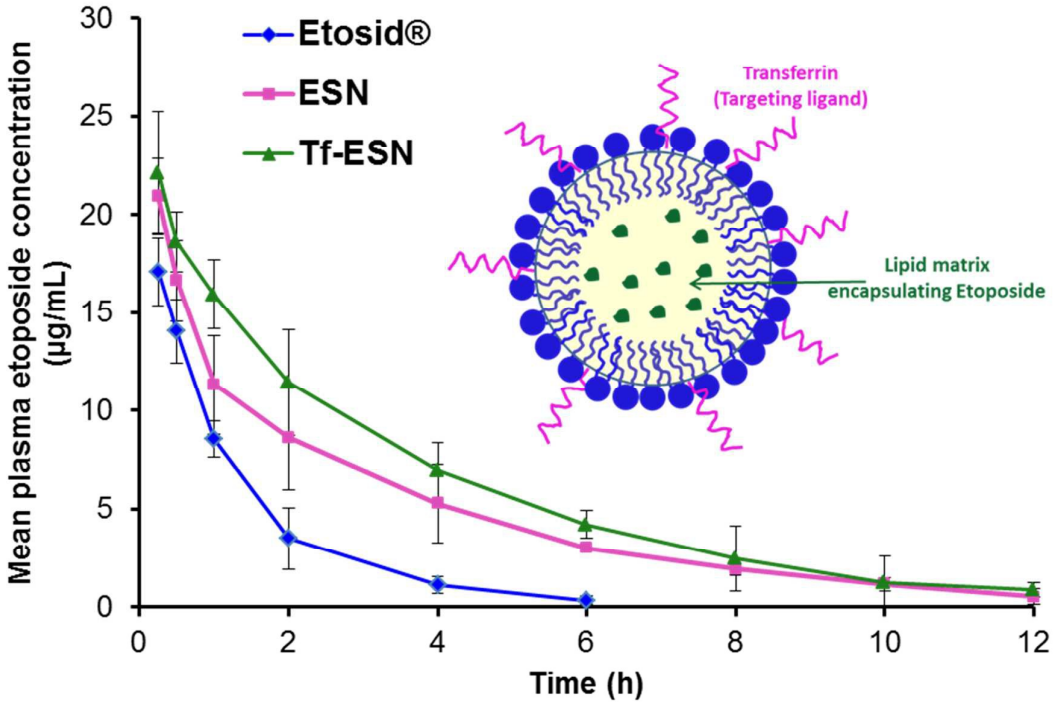

Cite this: DOI: 10.1039/c0xx00000x

www.rsc.org/xxxxxx

ARTICLE TYPE

Nanomedicines for targeted delivery of etoposide to non-small cell lung cancer using transferrin functionalized nanoparticles

Deep Pooja[a, b], Hitesh Kulhari[c,d], Lakshmi Tunki[a], Srinivas Chinde[e], Madhusudan Kuncha[a], Paramjit Grover[e], Shyam S Rachamalla[b], and Ramakrishna Sistla[a]*

Received (in XXX, XXX) Xth XXXXXXXXX 20XX, Accepted Xth XXXXXXXXX 20XX
DOI: 10.1039/b000000x

Abstract Lung cancer is the most common cause of cancer death. The clinical applications of anticancer drugs are limited due to non-specificity and systemic toxicity. Transferrin (Tf) receptors have been recognized to be up regulated in several malignant carcinomas including non-small cell lung cancer. Herein, we investigated the anticancer activity of Tf conjugated and etoposide (ETPS) loaded solid lipid nanoparticles (Tf-ESN) against Tf-receptors expressing A549 human non-small cell lung cancer cells. Pharmacokinetic and tissue-distribution profiles of nanoparticles were studied in Balb/c mice. Targeted nanoparticles showed significantly higher anticancer activity of etoposide manifested by anti-proliferation assay, morphological changes and induced apoptosis in A549 cells. In biodistribution studies, Tf-ESN had higher plasma concentration, longer blood circulation and decrease in clearance of encapsulated ETPS than Etosid®, a marketed formulation of etoposide. In conclusion, the promising results of this study suggested that targeting of nanomedicines to Tf-receptors, those are over expressed in non-small cell lung cancer could increase the therapeutic efficacy of lung cancer therapy.

1. Introduction

In 2012, The International Agency for Research on Cancer (IARC) of World Health Organization reported that lung cancer is the most commonly diagnosed and cause of death among all cancers. About 1.8 million (13% of total) new lung cancer cases were diagnosed and about 1.6 million (19.4% of total) deaths occurred due to lung cancer.[1] Chemotherapy, along with surgery and radiotherapy, is an important part of cancer treatment. However, chemotherapy often fails to improve patient mortality and compliance due to poor physicochemical properties of anticancer drugs and severe side effects on healthy tissues. In addition, development of resistance in cancer cells towards chemotherapeutic agent further decreases the efficacy of the treatment. [2,3]

Nano-medicines have shown potential in diagnosis, treatment and monitoring of cancer.[4] Nanotechnology based targeted drug delivery systems can deliver anticancer drugs selectively to cancer cells. Apart from site-specific delivery, nanomedicines also enhance plasma solubility and bioavailability, increase stability and provide controlled drug release. All these factors contribute to decrease in total dose requirements which lead to decrease in side-effects and improve patient compliance.[5,6]

Etoposide [4'-demethylepipodophyllotoxin-9-(4, 6-o-ethllidene-β-D-glycopyranoside)] (ETPS) is a semi-synthetic derivative of podophyllotoxin and has been approved by Food and Drug Administration for the treatment of small cell lung cancer and testicular carcinoma. ETPS has also shown significant cytotoxicity against Kaposi's sarcoma associated with AIDS, Hodgkin's and non-Hodgkins lymphoma, breast, gastric and ovarian cancers.[7-9] ETPS is a potent topoisomerase II inhibitor, enzyme responsible for unwinding of DNA helix. It acts in the G2 and S phases of cell cycle and prevents entry of cell into the mitotic phase of cell cycle leading to cell death.[10] Poor aqueous solubility, chemical instability and non-specific toxicities to normal tissues are the major limitations of ETPS in its clinical applications. [11,12] Currently, ETPS is being supplied as oral soft capsules and injection formulations.[12] However, non-aqueous, organic solvents and solubilizers such as benzyl alcohol, ethanol, polysorbate 80 and PEG 300 are being used to solubilize ETPS. These solubilizers frequently cause hypotension, anaphylaxis and bronchospasm.[8]

In this investigation, we developed transferrin conjugated solid lipid nanoparticles for the improved delivery of ETPS to lung cancer. Solid lipid nanoparticles (SLNs) contain solid lipid as matrix which are highly biocompatible and biodegradable. SLNs also have the advantages of high drug payload, increased drug

[a]Medicinal Chemistry & Pharmacology Division, CSIR-Indian Institute of Chemical Technology,Hyderabad-500007, India. Email: sistla@iict.res.in.
[b]Faculty of Pharmacy, University College of Technology, Osmania University, Hyderabad, India
[c]IICT-RMIT Joint Research Centre, CSIR-Indian Institute of Chemical Technology, Hyderabad – 500007, India.
[d]School of Applied Sciences, RMIT University, Melbourne–3000, Australia.
[e]Toxicology Unit, Biology Division, CSIR-Indian Institute of Chemical Technology, Uppal Road, Hyderabad – 500 607, India.

stability, large scale production and sterilization.[5,13] Transferrin (Tf), human-holo, was selected as targeting ligand. Tf is a single polypeptide glycoprotein consisting of about 679 amino acids. Tf has an important role in iron transport in the human body. Cancer cells require more iron for their rapid growth and proliferation which results in up regulation of Tf-receptors in several malignant tumors including lung, breast, brain, prostate, and colorectal cancers.[14-18] Tf has been recognised and explored as a potential targeting ligand for the delivery of drugs to brain and breast cancers.[17,19-23] However, its role against Tf-receptors over expressing lung cancer is not investigated. In this study, we demonstrate the anticancer activity of Tf-conjugated ETPS loaded SLNs (Tf-ESN) against Tf-receptors overexpressing A549 human lung cancer cells. In addition, we studied the pharmacokinetic and tissue distribution profiles of Tf-ESN in Balb/C mice in comparison to Etosid®, a marketed formulation of ETPS.

2. Experimental section

2.1. Materials

Glycerol monostearate (GMS) was purchased from Alfa Aesar (Johnson Matthey Chemicals, Hyderabad, India). Holo-transferrin, dimethyl sulfoxide (DMSO), RPMI-1640, trypsin–EDTA, antibiotic antimycotic solution, 3-(4, 5- dimethylthiazol-2-yl)-2, 5-diphenyl tetrazolium bromide (MTT), N-(3-dimethylaminopropyl)-N'-ethylcarbodiimide (EDC), N-hydroxysuccinimide (NHS) and stearic acid were purchased from Sigma Aldrich (St. Louis, MO, USA). Etoposide (ETPS) was a gift sample from TherDose Pharma Pvt. Ltd. (Hyderabd, India). A549 human non-small cell lung cancer cells were purchased from American Type Culture Collection (ATCC) (Manassas, VA, USA). Fetal bovine serum (FBS) was purchased from Gibco, USA. High performance liquid chromatography (HPLC) grade solvents were purchased from Merck specialties (Mumbai, India). Lecithin soya and dialysis tubing (molecular weight cut off 12000-14000) were obtained from of Himedia (Mumbai, India). Bradford reagent was purchased from Biomatik (Hyderabad, India). Tween 80 was purchased from sd Fine Chem. Ltd (Mumbai, India).

2.2. Preparation of etoposide loaded solid nanoparticles

ETPS loaded solid lipid nanoparticles (ESN) were prepared by single emulsification and solvent-evaporation method. ETPS (10 mg), GMS (85 mg), soya lecithin (40 mg) and stearic acid (15 mg) were dissolved in 2 mL of chloroform and poured in to 10 mL of 1.5% w/v of Tween® 80 solution. The dispersion was homogenized at 11000 rpm for 5 min and sonicated for 20 min. The mixture kept for stirring for 3 h. The nanoparticle dispersion was centrifuged at 15000 rpm for 45 min. Nanoparticles obtained as pellet and washed 3-4 times with milliQ water and lyophilized using trehalose dihydrate as cryoprotectant.

2.3. ETPS encapsulation efficiency

Encapsulation efficiency was determined by indirect method using a HPLC instrument (Waters, USA). The supernatant obtained after centrifugation of nanoparticle dispersion was used for the estimation of free drug content. Reverse-phase HPLC was performed using a C_{18} column (Waters Reliant, 5µm, 4.6 × 250 mm). The mobile phase, a mixture of methanol and water (50:50, v/v), was pumped at a flow rate of 1.0 ml/min, and UV detection was set at 224 nm. Drug encapsulation efficiency was determined as % Encapsulation efficiency = {1-(Ds/Di)} × 100, whereas Ds: Amount of drug in supernatant; Di: initial amount of drug added.

2.4. Surface conjugation of transferrin to ESN

The conjugation reaction was performed by EDC/NHS chemistry. Fifty mg of lyophilized ESN were dispersed in 5 mL of phosphate buffer saline pH 7.4 (PBS) and 1 mL of 1 mM EDC/NHS was added and stirred for 2 h. Thereafter, Tf was added and incubated for 8 h. Conjugation efficiency was determined by Bradford protein assay using microplate reader (Synergy 4, Biotek, USA) as described previously.[24]

2.5. Characterization of nanoparticles

The mean particle diameter, size distribution and zeta potential of various formulations i.e. BSN, ESN and Tf-ESN were determined by photon correlation spectroscopy using particles size analyzer Nano-ZS (Malvern instrument Ltd., Malvern, UK). Surface morphology of SLN was assessed by transmission electron microscopy. The formulation was placed on copper grid and allowed to dry. Dried sample was stained with 1% uranyl acetate solution and excess of reagent was removed by using filter paper. Nanoparticles were observed using a transmission electron microscope (JEOL, Japan).

The X-Ray diffraction patterns of ETPS, GMS, blank solid lipid nanoparticles (BSN), and ESN were measured with Bruker AXS D8 X-ray diffraction (Germany). The instrument was operated over 2θ range from 8 to 65°. DSC analysis was carried out to determine physical state of ETPS, before and after encapsulation in SLN by using DSC STAR ONE (Mettler, Switzerland). DSC thermograms of free ETPS, GMS, BSN and ESN were obtained by scanning the samples from 50 °C to 300 °C at a speed of 10 °C/min, under nitrogen environment. Fourier transform infrared analysis (FTIR) was performed by FTIR (Perkin elmer, Spectrum one) over the range of wave number 4000-450 cm^{-1}.

2.6. *In-vitro* drug release

In-vitro drug release behaviour of ETPS formulations was determined by dialysis bag method. Experiments were performed in PBS and sodium acetate buffer pH 5.0 (SAB) containing 0.5% w/v Tween 80. Briefly, ETPS, ESN and Tf-ESN, equivalent to 2 mg of ETPS drug, were placed into dialysis bag. The bag was kept in release medium and stirred at 100 rpm and temperature was maintained at 37±0.5 °C. One mL of aliquots was withdrawn at predetermined time intervals and replenished with the same volume of fresh buffer. Estimation of ETPS content in samples was performed by HPLC analysis.

2.7. Anti-proliferation assay

In-vitro cytotoxicity of native ETPS, ESN and Tf-ESN against A549 cells was evaluated by MTT assay. A549 human non-small cell lung cancer cells were cultured in RPMI-1640 medium supplemented with 10% FBS, 100 µg/mL streptomycin, 100 U/mL penicillin, and at 37 °C in a 5% CO_2 incubator. Cells (5×10^3 cells/well) were seeded in 96-well plate and incubated with different concentration of test formulations. After 48 h, media was replaced with serum-free media containing 0.5 mg/mL of MTT reagent and cells were incubated for 4 h. Then media was removed and formazan crystals generated by live cells were dissolved by adding 150 µL of DMSO in each well. The

absorbance was measured using a microplate reader at a wavelength of 570 nm. The relative cell viability (%) was determined by comparing the absorbance with control wells. Data are presented as average ± SD (n = 4).

2.8. Cellular uptake studies

In order to study the uptake of nanoparticles in A549 cells, Rhodamine-b loaded solid lipid nanoparticles (RSN) were prepared and then conjugated with Tf to give targeted, florescent nanoparticles (Tf-RSN) as described earlier. A549 cells (5×10^5) were seeded in 12-wells plate and allowed to adhere for 24 h. Thereafter, cells were incubated with RSN and Tf-RSN for different time intervals. Cells were washed three times with cold PBS, fixed with 4% paraformaldehyde and incubated with nucleus staining dye Hoechst (5 µg/mL) for 30 min at 37 °C. Cells were washed twice with PBS and fluorescent images were taken using a fluorescent microscope.

2.9. Cell morphology studies using acridine orange and ethidium bromide

A549 cells were cultured in 24-wells plate as a density of 5×10^5 cells per well. Cells were treated with ETPS, ESN and Tf-ESN (equivalent to 0.6 µg/mL of ETPS) for 24 h. Cells were rinsed with PBS and fixed with 4% paraformaldehyde for 10 min. Cells were stained with AO and EB solution containing 10 µg/mL of each. Cells were incubated for 15 min, washed with PBS and then observed using fluorescent microscope.

2.10. Apoptosis studies using Hoechst 33342

The *in-vitro* apoptosis induced by different ETPS formulation was assessed by Hoechst 33342 staining[11,36,37]. A549 cells were treated with ETPS, ESN and Tf-ESN (equivalent to 0.6 µg/mL of ETPS) for 24 h. Cells were washed with PBS and stained with Hoechst 33342 (5 µg/mL) for 30 min at 37 °C. Thereafter, cells were again washed three times with PBS to remove excess dye. The images were observed using fluorescence microscope.

2.11. Pharmacokinetic and bio-distribution study

Pharmacokinetic and biodistribution studies were carried out in BALB/c mice, weighing 20-25 g, in accordance with rules and regulation of CPCSEA, New Delhi, India. One hundred and eight animals were randomly divided into three groups. Each group received 10 mg/kg body weight at dose of pure etoposide via tail vein of Etosid®, ESN and Tf-ESN, respectively. A volume of 300 µL of blood and tissues of interest viz. spleen, lung, liver, kidney, brain and heart were collected at defined time points (0.25, 0.5, 1, 2, 4, 6, 8, 10, and 12 h). Plasma was collected by centrifuging blood at 5000 g for 10 min. Tissues were rinsed with PBS. Plasma and tissues were stored at -80 °C till further analysis.

Plasma and tissue samples processing and analysis.

For estimation of etoposide by HPLC, the tissues were thawed, weighed and homogenised in PBS (1:5 dilutions) using a tissue homogenizer (Heidolph, silent crusher S). Plasma (100 µL) or tissue homogenate (200 µL) was mixed with 10 µL of podophyllotoxin (internal standard) and vortexed for 30 sec. Thereafter, 1 mL of ethyl acetate was added, vortexed for 60 sec, and centrifuged at 8000 rpm for 10 min. The organic phase was collected and evaporated to dryness. The residue was reconstituted with mobile phase, 100 µL for plasma and 200 µL for tissue samples. A volume of 25 µL of reconstituted sample was injected into a HPLC system. Various pharmacokinetic parameters like maximum plasma concentration (C_{max}), plasma half life ($t_{1/2}$), area under the curve (AUC) and mean residence time (MRT) were determined by drug concentration versus time curve.

2.12. Statistical analysis

All the experiments were performed in triplicate (n=3) and data are shown as mean ± SD. Student t-test was used to determine the statistical difference, p value < 0.05 considered as significant.

3. Results and discussion

3.1. Preparation of etoposide loaded solid lipid nanoparticles (ESN)

SLNs were prepared by single emulsification and solvent-evaporation method. GMS was selected as solid lipid matrix while soy lecithin and Tween® 80 were chosen as co-surfactant and surfactant, respectively. Stearic acid was incorporated to create free carboxylic groups on the surface of nanoparticles. For the preparation of ESN, ETPS was dissolved in organic phase.

The average particle diameter was 54.6±2.5 nm and 66.9±4.1 nm for blank solid lipid nanoparticles (BSN) and ESN, respectively. The low polydispersity indexes (PDI) of nanoparticles indicated the uniformity of size of nanoparticles (Table 1). Zeta potential of BSN and ESN was -25.3±2.4 mV and -26.1±1.7 mV, respectively, suggesting high physical stability of nanoparticles.

3.2. Bioconjugation of Tf to ESN

Tf was conjugated to the surface ESN by two steps EDC/NHS reaction. In first step, carboxylic groups present on the surface of ESN were activated by addition of EDC and stabilized by NHS. In second step, activated carboxylic groups were allowed to interact with free amine groups present on Tf. The conjugation efficiency was determined by Bradford assay and found to be 71.8±4.6%. Tf-conjugated ESN (Tf-ESN) exhibited particles size of 96.7±3.4 nm, PDI 0.216 and zeta potential -17.5±2.9 mV (Fig. 1a). A significant decrease in negative zeta potential of Tf-ESN also confirmed the conjugation of Tf to ESN (Table 1).

Table 1. Physicochemical characterization of nanoparticles (Mean ± SD; n=6)

	PD (nm)	PDI	ZP (mV)	% EE	%DL	%CE
BSN	54.6 ±2.5	0.114 ±0.13	-25.3 ±2.4	--	--	--
ESN	66.9 ±4.1	0.194 ±0.09	-26.1 ±1.7	92.1 ±1.5	6.54 ±1.1	---
Tf-ESN	96.7 ±3.4	0.216 ±0.18	-17.5 ±2.9	85.9 ±2.3	6.08 ±1.3	71.8 ±4.6

BSN: Blank solid lipid nanoparticles; ESN: Etoposide loaded solid lipid nanoparticles; Tf-ESN: Transferrin conjugated ESN; PD: Particle diameter; PDI: Polydispersity index; ZP: Zeta potential; EE: Drug Encapsulation efficiency; DL: Drug loading; CE: Transferrin conjugation efficiency.

3.3. Physicochemical characterization

TEM is an useful technique to determine the shape and size of nanoparticles. TEM photomicrograph of Tf-ESN is shown in Figure 1b which revealed that nanoparticles were spherical in shape and in agreement with DLS results (Fig. 1a).

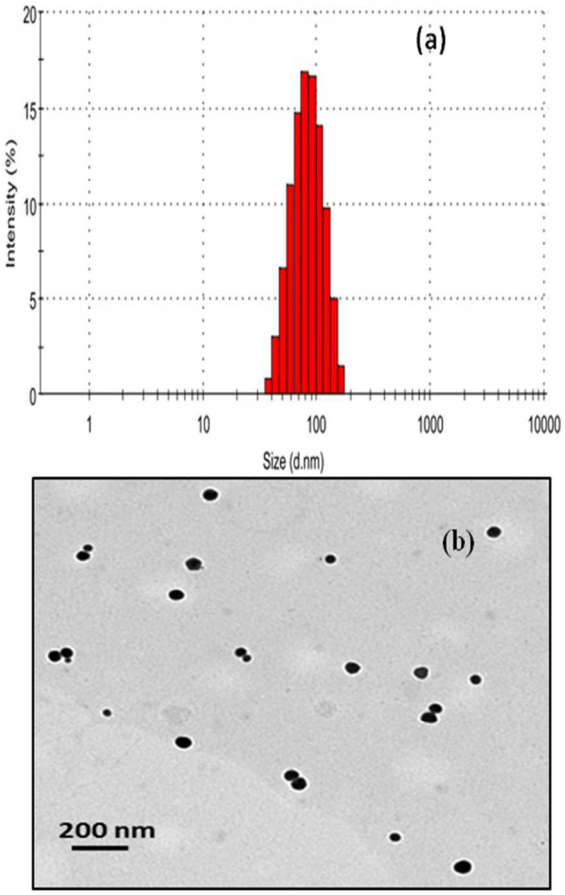

Fig. 1 a) Particle size and distribution of Transferrin conjugated and Etoposide loaded solid lipid nanoparticles (Tf-ESN) measured by DLS. b) TEM micrograph of Tf-ESN.

FTIR analysis was performed to confirm the surface conjugation of Tf to SLN (Fig. 2). FTIR spectra of ESN showed characteristic C=O stretching of carboxylic group of stearic acid at 1731 cm^{-1} which was not observed in Tf conjugated nanoparticles (Tf-ESN). In addition, a new peak at 1653 cm^{-1} was observed corresponding to amide bond formed between carboxylic groups of nanoparticles and amine groups of Tf.

XRD diffractogram of ETPS, GMS, BSN and ESN are shown in Fig. 3a. Two sharp peaks at 18 and 23° were observed in XRD diffraction patterns of GMS, suggesting crystalline nature of the lipid. These peaks were also observed, but less intense, in BSN and ESN diffractograms. The XRD pattern of ETPS showed characteristic sharp peaks from 2Θ angle 10 to 27°, confirming high crystalline state of pure ETPS. The aforementioned sharp peaks were absent in diffraction patterns of ESN which indicated that ETPS was present either in its amorphous form or was molecularly dispersed in solid lipid matrix of nanoparticles.

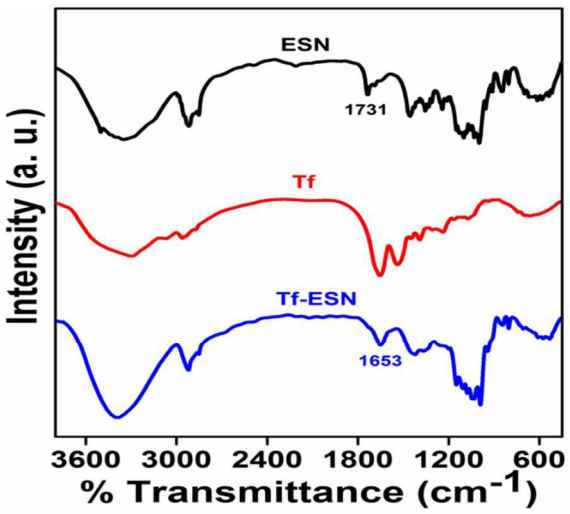

Fig. 2. FTIR spectra of Etoposide loaded solid lipid nanoparticles (ESN), Transferrin (Tf) and Tf-conjugated ESN (Tf-ESN)

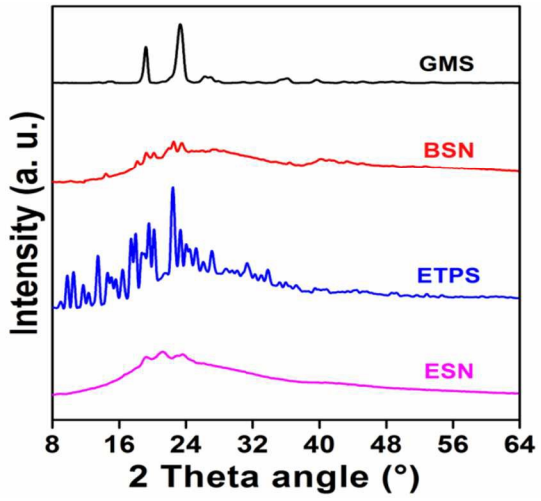

a)

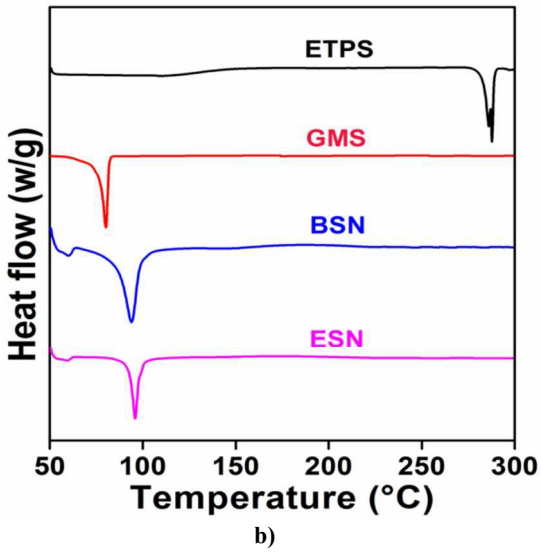

b)

Fig 3. a) X-Ray diffraction patterns and b) Diffrential scanning calorimetric analysis of GMS, BSN, pure etoposide and ESN.

The DSC scans of ETPS, GMS, BSN, and ESN were obtained to determine the physical state of ETPS and bulk lipid as pure compound and inside the nanoparticles (Fig. 3b). The spectra of pure ETPS exhibited a sharp peak at 287 °C demonstrating high crystalline nature of ETPS. Bulk GMS showed a characteristic melting endothermic peak at 76.5 °C. However, in case of BSN, GMS peak was shifted to 63 °C with a broad shouldering. It has been observed that lipids behave differently in bulk form and SLN formulations. [25,26] A shift in melting point of GMS in SLN formulations could also be explained by the small particle size of SLNs which results in high surface energy and presence of surfactant.[27,28] In addition, lattice defects are created during the preparation of SLN which lead to decrease in crystallinity of lipid in use. These less ordered crystalline or amorphous solids require less energy to melt than original crystalline substances and show a broad and less intense peak.[29] BSN showed a sharp peak at 97 °C which is due to presence of trehalose dihydrate as cryoprotectant.[30] As trehalose dihydrate was incorporated after formulation of SLN, it was present in its crystalline state in final formulation. The DSC thermogram of ESN showed a broad peak of GMS and a sharp peak of trehalose dehydrate similar to BSN. Moreover, ETPS peak was not observed in the spectra of ESN which indicated a transformation of crystalline ETPS to its amorphous form.

3.4. *In-vitro* drug release of ETPS from different formulations

In vitro drug release studies were performed for pure ETPS, ESN and Tf-ESN in two media, PBS and SAB to determine the pattern and mechanism of release of drug from nanoparticles. From pure ETPS suspension, drug was released completely within 10 h in both media (Table 2). In case of ESN and Tf-ESN, a biphasic release pattern was observed in both the media. After initial burst release (~25% of entrapped drug within first 3 h), both nanoparticle-mediated formulations showed sustained release of drug up to 72 h.

Table 2a. In vitro drug release profiles ETPS, ESN and Tf-ESN in phosphate buffer saline pH 7.4 (PBS).

Time (h)	ETPS	ESN	Tf-ESN
6	71.9±1.4	35.1±1.6	37.9±2.2
10	98.7±0.9	44.2±2.5	49.6±1.7
24		56.7±1.7	61.7±1.4
48		64.8±2.2	72.4±2.2
72		76.2±2.8	81.8±2.5

Table 2b. In vitro drug release profiles ETPS, ESN and Tf-ESN in sodium phosphate buffer pH 5.0 (SAB).

Time (h)	ETPS	ESN	Tf-ESN
6	79.4±3.0	38.6±2.7	41.9±2.6
10	99.3±0.6	47.8±1.5	53.3±1.1
24	--	64.9±3.0*	68.9±2.2#
48	--	73.2±2.5*	76.9±2.4#
72	--	84.3±2.6*	88.4±1.7#

*Statistical analysis: * and # p value <0.05*

** indicates the comparison of drug release of ESN in PBS and SAB while # indicates the comparison of drug release of Tf-ESN in PBS and SAB.*

This kind of drug release behaviour is quite common because drug present in the peripheral shell or on the nanoparticle surface is released at a faster rate than the drug present inside the lipid core of nanoparticles.[31,32] However, there was no significant difference ($p>0.05$) in the release of drug from ESN and Tf-ESN which suggested that conjugation of Tf on the surface of nanoparticles does not interfere in the release of drug from nanoparticles. A significant difference ($p<0.05$) at 24, 48 and 72 h, was observed between release of ETPS from ESN and Tf-ESN in SAB media. A faster release of drug in media with acidic pH may help in more drug release in cancer cells those are having less pH than normal healthy cells.

3.5. Induction of cytotoxicity

The *in-vitro* anticancer efficacy of three ETPS formulation against A549 human lung cancer cells was investigated by anti-proliferation assay. Fig. 4 shows the cell viability results for cells treated with ETPS, ESN and Tf-ESN at concentration range 0.01-100 µg/mL. The cell viability was highest for the cells treated with ETPS followed by ESN and Tf-ESN. The observed IC_{50} value for ETPS, ESN and Tf-SLN was 2.01, 0.762 and 0.303 µg/mL; respectively. A statistical significant difference was observed in the concentration from 0.1-10 µg/mL. Insignificant difference ($p>0.05$) was observed at very low and high concentration which may be due that at low concentration amount of drug delivered by nanoparticles was not superior to that reaching in case of pure ETPS solution. Similarly at very high concentration, at drug provided by pure ETPS was sufficient to produce similar cell-killing effect to the amount of drug provided by formulation. The results suggested that plain ETPS has low anticancer activity against A549 cells. However, its activity was increased up to 6.6 times after encapsulation into SLNs. Blank nanoparticles showed more than 94% cell viability at all tested concentrations which confirmed that SLNs are highly biocompatible as drug carrier and the toxicity of ESN was due to ETPS delivered by the nanoparticles. Further, the lower viability of cells treated with Tf-ESN than cells treated with ESN indicated that the conjugation of Tf on the surface of SLNs enhanced the cytotoxicity of ETPS nanoparticles.

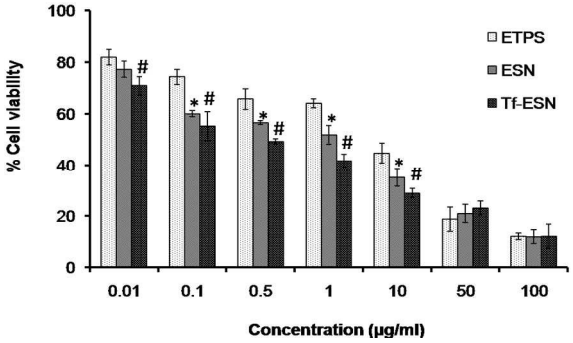

Fig. 4. Anti-proliferation assay: Percentage of cell viability of A549 human lung cancer cells after 48 h of treatment with pure etoposide (ETPS), ETPS loaded solid lipid nanoparticles (ESN) and Transferrin conjugated ESN (Tf-ESN).

*Statistical analysis: * and # p value <0.005*

** indicates comparison of cell viability of ESN with ETPS, while # indicates the comparison of cell viability of Tf-ESN with ETPS.*

3.6. Cellular uptake study

The uptake of fluorescent Rho-b loaded SLN (RSN) and Tf conjugated RSN (Tf-RSN) by A549 cells was visualized by fluorescence microscopy. It was observed that cells incubated with targeted Tf-SLN exhibited higher florescence intensity than non-targeted RSN (Fig. 5). The high fluorescence intensity of Rh-b with Tf-RSN could be attributed to enhanced internalization of Tf-RSN through Tf-receptors. Tf receptors have been found to over express in cancer cells including non-small cell lung cancer. Previous reports have demonstrated that Tf-conjugated nanoparticles had higher intracellular accumulation of encapsulated cargos, either drugs or fluorescent molecules, in Tf-receptors over expressing cancer cells than unconjugated nanoparticles.[17,19,.33] Tsuji et al., demonstrated that Tf-conjugated nanoparticles enter in cancer cells through clathrin-mediated endocytosis.[34] Therefore, the enhanced uptake of nanoparticles could be attributed to active targeting of Tf-RSN through Tf-receptors.

3.7. Cell morphology studies

To study the morphological changes in A549 cells after incubation with ETPS formulations, cells were labelled with AO and EB dyes. The permeability differences between two dyes provide a scope to differentiate live cells from dead cells. AO can permeate across the cell membrane of live cells while EB infiltrate only through damaged cell membrane of dead cells.

Therefore, live cells are stained by AO and appear with green florescence while dead cells exhibit orange to red fluorescence.

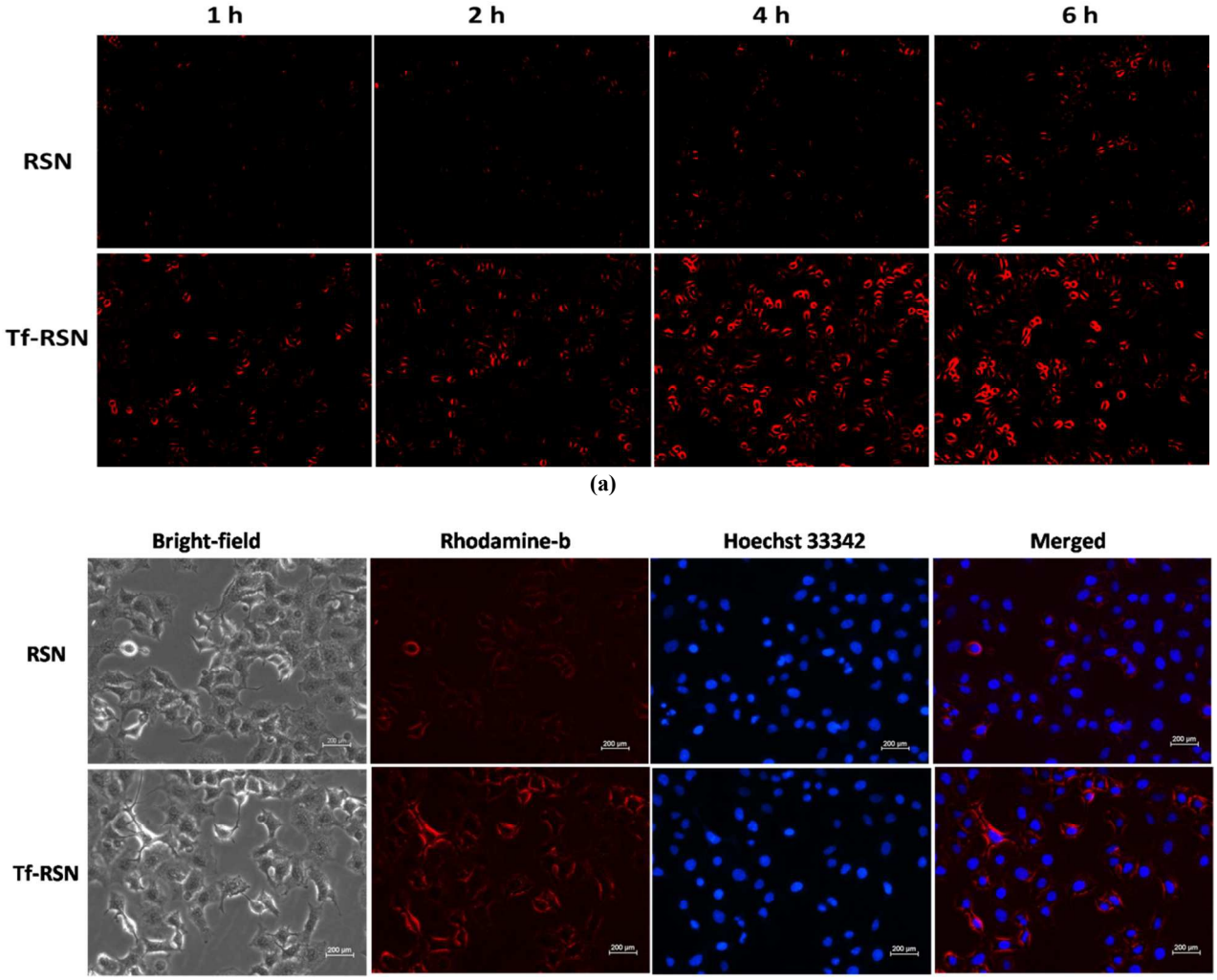

Fig. 5. Cell uptake studies: Fluorescent microscopic images of A549 human non-small cell lung cancer cells after incubation with Rhodamine-b loaded solid lipid nanoparticles (RSN) and Transferrin conjugated RSN (Tf-RSN). Both RSN and Tf-RSN incubated cells showed time-dependent uptake of nanoparticles (Figure 5a). However, Tf-RSN showed significantly higher florescence intensity, hence higher uptake than RSN. Figure 5b shows the images after 4 h at higher magnification. To visualize the nucleus, cells were stained with Hoechst 33342.

Fig. 6a shows the fluorescent microscopy images of untreated A549 cells (control) and the cells treated with ETPS, ESN and Tf-ESN. As expected, high green fluorescence was observed in control cells showing high cell viability. However, the number of live cells was decreased with three ETPS formulations, with a lowest number of viable cells in Tf-SLN group.

3.8. Apoptosis studies

Etoposide-induced cytotoxicity to the A549 cells was studied using nucleus staining dye Hoechst 33342. A549 cells were treated with ETPS, ESN and Tf-ESN for 24 h and then stained with Hoechst. Cells were observed for apoptotic characteristics Tf-ESN-treated cells showed more apoptotic nuclei than ETPS and ESN-treated cells. The results were consistent with anti-proliferation assay and suggested that modification of nanoparticles with Tf facilitated cellular uptake and accordingly enhanced apoptosis.

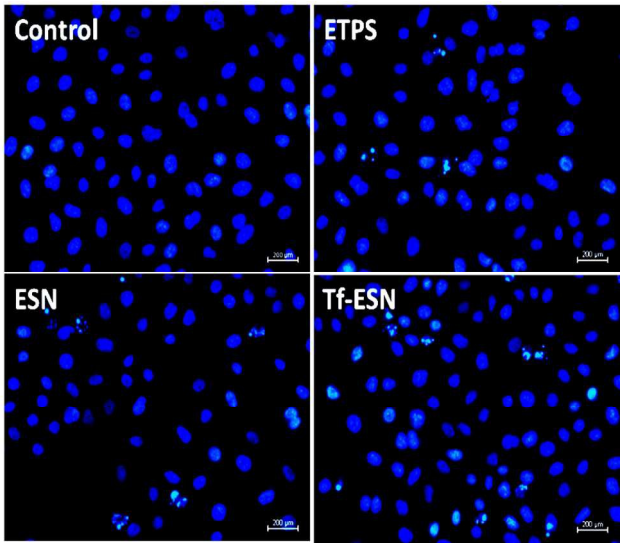

(a)

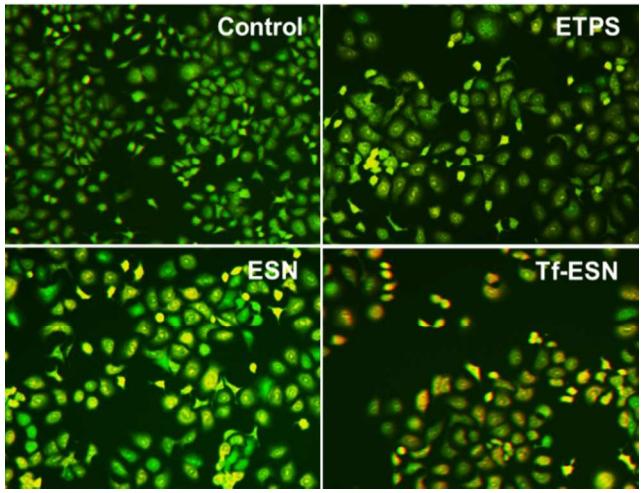

(b)

Fig. 6. Figure 6a demonstrates the morphology of A549 cells after 24 h of incubation with ETPS, ESN, and Tf-ESN containing 0.6 µg/mL ETPS. To differentiate viable cells from apoptotic or dead cells, cells were staines acridine orange and ethidium bromide**.** Figure 6b shows the **i**nduction of apoptosis in A549 human lung cancer cells after 24 h of treatment with pure etoposide (ETPS), ETPS loaded solid lipid nanoparticles (ESN) and Transferrin conjugated ESN (Tf-ESN).

3.9. In vivo pharmacokinetics and tissue distribution

such as cell shrinkage, nuclear fragmentation and apoptotic body formation. Untreated or control cells exhibited spherical and intact nuclei (Fig. 6b). ETPS-induced apoptosis was observed.

To study the in vivo behaviour of prepared nano-formulations, pharmacokinetic and tissue distribution of Etosid®, ESN and Tf-ESN were studied after intravenous administration in mice at a dose of 10 mg/Kg body weight. The profiles of plasma ETPS concentration versus time for three formulations are shown in Fig. 7 and calculated pharmacokinetic parameters are presented in Table 3. Following intravenous administration, the maximum plasma ETPS concentration was 17, 20.9 and 22.1 µg/mL for Etosid®, ESN and Tf-ESN, respectively after 15 min of administration. However, ETPS concentration was rapidly decreased in Etosid® treated mice as compared to ESN and Tf-ESN-treated mice. At all the time points, ETPS concentration was higher for nanoparticles formulations than Etosid®. It can be explained by the differences in nature of dosage forms. Etosid® is a solution formulation and rapidly distributes in other body tissues compared to ESN and Tf-ESN. Another side, ESN and Tf-ESN are nanoparticles formulations where drug is encapsulated in a lipid matrix that provides a sustained release of drug. There was a significant difference ($p<0.05$) between the plasma $AUC_{0-\infty}$ values of ETPS in Etosid® and ETPS delivered by both nanoparticle formulations as well as between the two nanoparticle formulations. The difference between AUC_{0-t} of ESN and Tf-ESN may be due to presence of Tf in Tf-ESN. It was quite interesting because no significant difference was observed in release of drug from two formulations during *in-vitro* drug release studies. It could be due to interaction of Tf with other blood components like serum proteins during pharmacokinetic studies that are absent in PBS used in *in-vitro* drug release studies. Results also indicated that Tf-conjugated nanoparticles had longer systemic circulation and slower plasma elimination rate than Etosid®. The MRT for Etosid®, ESN and Tf-ESN were 1.69, 3.63 and 3.74 h; respectively. The clearance of ETPS was significantly decreased with nanoparticle formulations when compared with Etosid®.

Table 3. Pharmacokinetic parameters of ETPS after administering as Etosid®, ETPS loaded solid lipid nanoparticles (ESN) and transferrin conjugated ESN (Tf-ESN) in BALB/c mice intravenously (Mean ±SD, n=4).

Pharmacokinetic Parameter	Etosid®	ESN	Tf-ESN
AUC_{0-t} (µg/mL/h)	22.16±3.1	59.38±7.2	73..32±5.3*
$AUMC_{0-\infty}$	37.57±5.2	216.02±19.1	274.91±14.8**
$t_{1/2}$ (h)	1.03±0.09	2.51±0.23	2.56±0.19**
Cl (mL/h)	452.4±22.7	168.38±11.2	136.9±13.8*
MRT (h)	1.69±0.1	3.53±0.28	3.74±0.34*

AUC: Area under the curve; AUMC: Area under moment curve; $t_{1/2}$: Plasma half life; Cl: Total clearance; MRT: Mean residence time

Statistical analysis: Results of final formulation Tf-ESN were compared with Etosid®.

* indicates $p<0.05$ and ** $p<0.005$.

The tissue distribution of ETPS from Etosid®, ESN and Tf-ESN is shown in Table 4. The results demonstrated that ETPS in Etosid® was maximum distributed to liver and least in brain. The

distribution order for ETPS encapsulated in ESN was lung>spleen>kidney>liver>heart and brain. A similar distribution pattern was observed for Tf-ESN. However, ETPS delivered by Tf-ESN was more in lung and brain while less in kidney, liver and spleen than ESN. There was no statistical difference ($p>0.05$) between ESN and Tf-ESN in delivery of ETPS to the heart. However, both ESN and Tf-ESN showed a significant decrease in the delivery of drugs to the heart as compared to Etosid®. This could be advantageous to decrease the cardiotoxicity of ETPS.[35] Both non-targeted ESN and targeted Tf-ESN nanoparticles showed more accumulation of ETPS in lungs which could help in the selective delivery of drugs for the treatment of lung cancer.

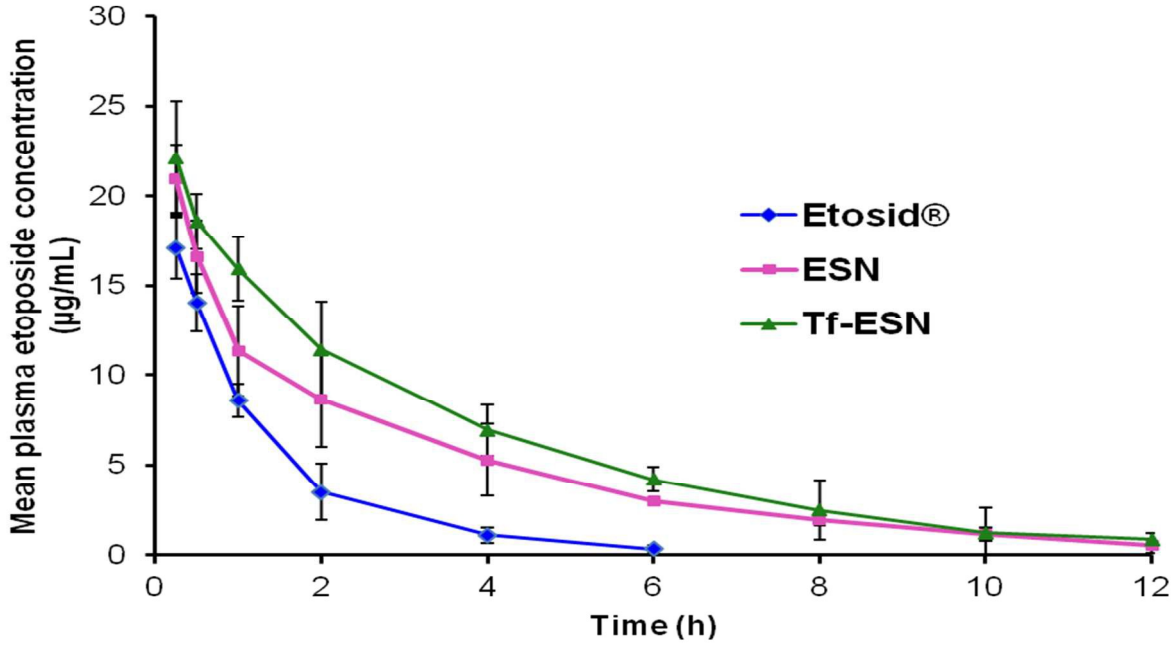

Fig. 7 Mean plasma etoposide concentration-time profile of Etosid®, ESN and Tf-ESN after intravenous administration at a dose of 10 mg/Kg body weight in Balb/c mice.

Table 4. Area under the curve (AUC), mean residence time (MRT) and half-life ($t_{1/2}$) of etoposide (ETPS) in various tissues after intravenous administration of Etosid®, ETPS loaded solid lipid nanoparticles (ESN) and transferrin conjugated ESN (Tf-ESN) in BALB/c mice (n=4).

Tissue	Etosid®			ESN			Tf-ESN		
	AUC	MRT	$t_{1/2}$	AUC	MRT	$t_{1/2}$	AUC	MRT	$t_{1/2}$
Lung	32.92	4.58	3.12	66.21	8.84	6.58	76.15	9.26	6.39
Liver	46.19	7.26	5.2	26.93	4.64	3.16	20.18	4.33	2.99
Spleen	33.07	4.4	3.04	31.4	4.8	3.2	23.14	4.2	2.68
Kidney	29.13	3.65	2.22	29.6	4.4	2.95	21.46	4.23	2.7
Heart	34.4	7.9	5.63	18.14	4.08	2.86	14.65	3.65	2.36
Brain	4.42	1.39	0.9	7.89	1.74	1.09	10.78	5.64	3.96

4. Conclusions

In summary, Tf-conjugated solid lipid nanoparticles were successfully prepared and characterized for targeting of ETPS to the A549 human non-small cell lung cancer cells. Tf-mediated internalization of Tf-ESN enhanced the anticancer activity and apoptosis of ETPS against tumor cells. Encapsulation of drug in the lipid matrix and conjugation of Tf on the surface of nanoparticles resulted in sustained drug release, improved plasma concentration and accumulation of ETPS in targeted lung tissues. Collectively, the prepared drug delivery system has the potential to target ETPS and, hopefully, other anticancer drugs effectively against lung carcinoma.

Acknowledgements

Authors thank to Director, CSIR-Indian Institute of Chemical Technology, Hyderabad for providing the necessary facilities and moral support. Authors are highly grateful to M/s Therdose Pharma for providing ETPS. H.K. is thankful to Director, IICT-RMIT Research centre for providing the Junior Research

Fellowship. D.P. thanks to Council of Scientific and Industrial Research (CSIR), New Delhi for awarding Senior Research fellowship. This work was financially supported by CSIR grant under project Advanced Drug Delivery Systems (ADD-CSC 0302).

References

1. Cancer, I. A. f. R. o., *World Health Organization* 2013, *223*, 1.
2. S. Kunjachan, B. Rychlik, G. Storm, F. Kiessling and T. Lammers, *Adv. Drug Del. Rev.*, 2013, *65*, 1852.
3. N. R. Patel, B. S. Pattni, A. H. Abouzeid and V. P. Torchilin, *Adv. Drug Del. Rev.*, 2013, *65*, 1748.
4. M. E. Davis, *Nat. Rev. Drug Discov.*, 2008, *7*, 771.
5. H. Harde, M. Das and S. Jain, *Expert Opin. Drug Del.*, 2011, *8*, 1407.
6. N. Sanvicens and M. P. Marco, Trends Biotechnol, 2008, *26*, 425.
7. K. Hande, *Eur. J. Cancer*, 1998, *34*, 1514.
8. F. Zhang, G. Y. Koh, J. Hollingsworth, P. S. Russo, R. W. Stout and Z. Liu, *Int. J. Pharm.*, 2012, *434*, 453.
9. I. A. Najar and R. K. Johri, *J Biosciennce*, 2014, *39*, 139.
10. C. Nam, K. Doi and H. Nakayama, *Histol Histopathol*, 2010, *25*, 485.
11. G. Yordanov, R. Skrobanska and A. Evangelatov, *Colloids Surf B*, 2013, *101*, 215.
12. N. Akhtar, S. Talegaonkar, R. K. Khar and M. Jaggi, *Saudi Pharm J*, 2013, *21*, 103.
13. W. Mehnert and K. Mader, *Adv. Drug Del. Rev.,* 2001, 47 (2), 165.
14. A. Widera, F. Norouziyan and W. C. Shen, *Adv. Drug Del. Rev.*, 2003, *55*, 1439.
15. J. F. Whitney, J. M. Clark, T.W. Griffin, S. Gautam and K. O. Leslie, *Cancer*, 1995, *76*, 20.
16. J. M. Vidal, M. Koulibaly, J. L. Jost, J. J. Duron, J. P. Chigot, P. Vayre, A. Aurengo, J. C. Legrand, G. Rosselin and C. Gespach. *Int. J. Oncol*., 1998, *13*, 871.
17. Y. Zheng, B. Yu, W. Weecharangsan, L. Piao, M. Darby, Y. Mao, R. Koynova, X. Yang, H. Li and S. Xu, *Int. J. Pharm.*, 2010, *390*, 234.
18. S. Kukulj, M. Jaganjac, M. Boranic, S. Krizanac, Z. Santic and M. Poljak-Blazi, *Med. Oncol.,* 2010, *27*, 268.
19. C. W. Gan and S. S. Feng, *Biomaterials*, 2010, *31*, 7748.
20. Y. Cui, Q. Xu, P. K. H. Chow, D. Wang and C. H. Wang, *Biomaterials*, 2013, *34*, 8511.
21. F. Yan, Y. Wang, S. He, S. Ku, W. Gu and L. Ye, *J. Mater. Sci.- Mater. Med.*, 2013, *24*, 2371.
22. M. Porru, S. Zappavigna, G. Salzano, A. Luce, A. Stoppacciaro, M. L. Balestrieri, S. Artuso, S. Lusa, G De Rosa, C. Leonetti and M. Caraglia, *Oncotarget*, 2014, *5*, 10446.
23. S. K. Sahoo and V. Labhasetwar, *Mol. Pharm.*, 2005, *2*, 373.
24. H. Kulhari, D. P. Kulhari, M. K. Singh and R. Sistla, *Colloids Surf. A*, 2014, *443*, 459.
25. A. Kovacevic, S. Savic, G. Vuleta, R. Muller and C. Keck, *Int. J. Pharm.*, 2011, *406,* 163.
26. S. Das, W. K. Ng and R. B. Tan, *Eur. J. Pharm. Sci.*, 2012, *47*, 139.
27. K. Vivek, H. Reddy and R. S. Murthy, *AAPS PharmSciTech*, 2007, 8 (4), 16.
28. V. Venkateswarlu and K. Manjunath, *J. Control. Release*, 2004, *95*, 627.
29. A. P. Nayak, W. Tiyaboonchai, S. Patankar, B. Madhusudhan and E. B. Souto, *Colloids Surf. B*, 2010, *81*, 263.
30. L. S. Taylor and P. York, *J. Pharm. Sci.*, 1998, *87*, 347.
31. J. Sun, C. Bi, H. M. Chan, S. Sun, Q. Zhang and Y. Zheng, *Colloids Surf. B*, 2013, *111*, 367.
32. S. Jose, S. S. Anju, T. A. Cinu, N. A. Aleykutty, S. Thomas and E. B. Souto, *Int. J. Pharm.*, 2014, *474*, 6.
33. J. L. Li, L. Wang, X. Y. Liu, Z. P. Zhang, H. C. Guo, W. M. Liu and S. H. Tang, *Cancer Lett*, 2009, *274*, 319.
34. T. Tsuji, H. Yoshitomi and J. Usukura, *Microscopy (Oxf)*, 2013, *62*, 341.
35. J. D. Floyd, D. T. Nguyen, R. L. Lobins, Q. Bashir, D. C. Doll and M. C. Perry, *J. Clin. Oncol.*, 2005, *23*, 7685.
36. R. Vivek, V. N. Babu, R. Thangam. K.S. Subramanian and S. Kannan, *Colloids Surf B*, 2013, *111*, 117.
37. Z. Li, L. Qiu, Q. Chen, T. Hao, M. Quio, H. Zhao, J. Zhang, H. Hu, X. Zhao, D. Chen and L. Mei, *Acta Biomater*, 2015,*11*, 137.